Simulations of Hydrogen, Carbon Dioxide, and Small Hydrocarbon Sorption in a Nitrogen-Rich *rht*-Metal–Organic Framework

Douglas M. Franz[†], Zachary E. Dyott[†,‡], Katherine A. Forrest[†], Adam Hogan[†], Tony Pham[*,†], and Brian Space[*,†]
[†]*Department of Chemistry, University of South Florida,*
4202 East Fowler Avenue, CHE205, Tampa, FL 33620-5250, United States
[‡]*Theoretical Chemistry Institute, Department of Chemistry, University of Wisconsin-Madison,*
1101 University Avenue, Madison, WI 53706, United States
[*]brian.b.space@gmail.com; tpham4@mail.usf.edu

Grand Canonical Monte Carlo

Simulations of hydrogen sorption in Cu-TDPAH, also known as *rht*-MOF-9, hereafter [**1**], were performed using grand canonical Monte Carlo (GCMC) on a single unit cell ($27.934 \times 27.934 \times 41.081$ Å^3) of the MOF. This method constrains the chemical potential (μ), volume (V), and temperature (T) of the MOF–sorbate system to be constant while allowing other thermodynamic quantities to fluctuate.[1] The simulation involves randomly inserting, deleting, translating, or rotating a sorbate molecule with acceptance or rejection based on a random number generator scaled by the energetic favorability of the move. An infinitely extended crystal environment was approximated by periodic boundary conditions with a spherical cut-off corresponding to half the shortest unit cell dimension length ($a = b = 27.934$ Å). All MOF atoms were constrained to be rigid for the simulations. In GCMC, the average particle number was calculated by the following expression:[2,3]

$$\langle N \rangle = \frac{1}{\Xi} \sum_{N=0}^{\infty} e^{\beta \mu N} \left\{ \prod_{i=1}^{3N} \int_{-\infty}^{\infty} dx_i \right\} N e^{-\beta U(x_1, \ldots x_{3N})} \tag{1}$$

where Ξ is the grand canonical partition function, β is the quantity $1/kT$ (k is the Boltzmann constant), and U is the total potential energy. The chemical potential for hydrogen was determined using the BACK equation of state.[4] The total potential energy of the MOF–sorbate system was calculated by summing the repulsion/dispersion energy, the electrostatic energy, and the many-body polarization energy. Once $\langle N \rangle$ was calculated, it was converted to a value that can be compared with experiment, which is weight percent (wt %) in this case, defined as: [(Mass of sorbates)/(Mass of MOF + Mass of sorbates)] $\times$ 100% for H_2, or mmolg^{-1} for all other sorbates.

For the simulations of hydrogen sorption at the temperatures considered in this work, quantum mechanical dispersion effects were included semiclassically through the fourth order Feynman-Hibbs correction according to the following equation:[5]

$$U_{FH} = U + \frac{\beta \hbar^2}{24\mu} \left(U'' + \frac{2}{r} U' \right) + \frac{\beta^2 \hbar^4}{1152 \mu^2} \left(\frac{15}{r^3} U' + \frac{4}{r} U''' + U'''' \right) \tag{2}$$

where $\hbar$ is the reduced Planck's constant and the primes indicate differentiation with respect to pair separation r.

The isosteric heat of adsorption (Q_{st}) values were calculated based on the fluctuations in the particle number and the total potential energy in the system through the following expression:[6]

$$Q_{st} = -\frac{\langle NU \rangle - \langle N \rangle \langle U \rangle}{\langle N^2 \rangle - \langle N \rangle^2} + kT \tag{3}$$

For all state points considered, the simulations consisted of a minimum of 2.5×10^5 Monte Carlo (MC) steps to guarantee equilibration. All simulations used a correlation time of 1×10^3 MC steps in order to produce uncorrelated equilibrium configurations. All simulations were performed using the Massively Parallel Monte Carlo (MPMC) code, which is currently available for download on GitHub[7]. Some validation and comparison was considered for isotherms and binding sites using Monte Carlo / Molecular Dynamics (MCMD)[8], another code developed in our lab.

Many-Body Polarization

An overview of the Thole-Applequist type polarization model[9–11] used in this work is given here. The induced dipole, μ, at site i can be calculated using the following equation:

$$\vec{\mu}_i = \alpha_i^{\circ} \left(\vec{E}_i^{stat} - \sum_{j \neq i}^{N} \mathbf{T}_{ij} \vec{\mu}_j \right) \tag{4}$$

where α_i° represents the atomic point polarizability, $\vec{E}_i^{stat}$ is the static electric field felt at site i due to the presence of the MOF atoms and the sorbate molecules, $\vec{\mu}_j$ represents the induced dipole at site j, and $\mathbf{T}_{ij}^{\alpha\beta}$ is the dipole field tensor which is defined from first-principles as the following:[9]

$$\mathbf{T}_{ij}^{\alpha\beta} = \nabla^{\alpha} \nabla^{\beta} \frac{1}{r_{ij}} \tag{5}$$

$$= \frac{\delta^{\alpha\beta}}{r_{ij}^3} - \frac{3 x^{\alpha} x^{\beta}}{r_{ij}^5} \tag{6}$$

where r_{ij} is the distance between sites i and j. Equation 4 is a self-consistent field equation with respect to the dipoles and thus, the quantity $\vec{\mu}_i$ must be solved for using iterative methods for large systems. The iterative method employed herein was the Gauss–Seidel relaxation technique.[12] This method consists of updating the current dipole vector set for the k^{th} iteration step as the new dipole vectors become available *via* the following:[13]

$$\vec{\mu}_i^k = \alpha_i^{\circ} \left(\vec{E}_i^{stat} - \sum_{j \neq i} \hat{T}_{ij} \vec{\mu}_j^{k-1+\zeta} \right) \tag{7}$$

$$\zeta = \begin{cases} 0, & \text{if } i < j \\ 1, & \text{if } i > j \end{cases} \tag{8}$$

In this equation, $\hat{T}_{ij}$ is the modified dipole field tensor that accounts for short range divergences in the polarization model, defined as:[13–15]

$$\hat{T}_{ij}^{\alpha\beta} = \frac{\delta_{\alpha\beta}}{r_{ij}^3} \left[1 - \left(\frac{\lambda^2 r_{ij}^2}{2} + \lambda r_{ij} + 1 \right) e^{-\lambda r_{ij}} \right] - \frac{3 x^{\alpha} x^{\beta}}{r_{ij}^5} \left[1 - \left(\frac{\lambda^3 r_{ij}^3}{6} + \frac{\lambda^2 r_{ij}^2}{2} + \lambda r_{ij} + 1 \right) e^{-\lambda r_{ij}} \right] \tag{9}$$

where λ is a parameter damping the dipole interactions near the regions of discontinuity. A value of 2.1304 was used for λ in this work, which is consistent with the work performed by B. Thole.[10] The many-body polarization energy for the MOF–sorbate system was calculated by the following based on the work of Palmo and Krimm:[16]

$$U_{pol}^k = -\frac{1}{2} \sum_i \vec{\mu}_i^k \cdot \vec{E}_i^{stat} - \frac{1}{2} \sum_i \vec{\mu}_i^k \cdot \vec{E}_i^{k+1} \tag{10}$$

Thus, the polarization energy was determined from the k^{th} iteration dipoles and the $(k+1)^{th}$ induced field. In the case of simulations of sorbates in [**1**] with polar models, k was equal to 4.

All molecular visualizations were rendered using Visual Molecular Dynamics[17].

Simulated Annealing

Simulated annealing calculations were performed on the MOF–sorbate systems at various starting temperatures using all models cited in the main text, with a starting temperature of 700 K. A generalized procedure for simulated annealing is provided by Kirkpatrick *et al.*[18] In this work, the temperature was scaled exponentially by a factor of 0.9999 after every 1 $\times$ 10^3 Monte Carlo steps. The starting positions of the sorbate molecules were located at random positions in the unit cell.

Methods for C_2 Hydrocarbon Model Development

C_2H_2, C_2H_4, and C_2H_6 were approximated as rigid molecules. The bond distances and angles used in the models were obtained from a geometry optimization at the CCSD(T)/aug-cc-pVQZ level of theory[19] with the electronic structure program ORCA.[20] The partial charges for the atoms on the C_2H_2, C_2H_4, and C_2H_6 molecules were obtained using the CHELPG method[21] on the orbital optimized CCSD/aug-cc-pVQZ electronic density[22] as implemented in ORCA. For polarizable potentials for the respective sorbates, scalar point polarizabilites on the atoms were obtained with the default procudure implemented by the CamCASP program.[23] Briefly, the molecular orbitals of the individual gas phase monomers were calculated at the PBE0/aug-cc-pVQZ level of theory with the CS00 asymptotic correction[24] as implemented in NWChem.[25] The total molecular polarizability and point-to-point polarizabilities between 2,000 points located on the 2x to 4x van der Waal surface were then calculated with the CKS propagator. These molecular polarizabilities were transformed to atom-centered polarizabilities using the localization procedure of Le Sueur and Stone.[26]

In order to obtain the Lennard-Jones 12-6 parameters, 1,000 randomized dimer configurations of C_2H_2, C_2H_4, and C_2H_6 were generated with 100 configurations for each gas, at each center-of-mass distance, starting at 3 Å through 13 Å, at evenly spaced intervals of 0.1 Å. Single point energies were then calculated for each dimer configuration at the CCSD(T)/CBS limit with a aug-cc-pVDZ/aug-cc-PVTZ extrapolation[27] and basis set superposition error was corrected by the counterpoise method.[28] Simulated annealing[18] was then used to optimize the Lennard-Jones parameters on the atomic sites, keeping all other previously calculated parameters constant; these calculations were performed with the MPMC code.[7] The parameters for the electrostatic and polarizable C_2H_2, C_2H_4, and C_2H_6 potentials used in this work are provided in Tables S6, S7, and S8, respectively.

[1] Unit Cell

Figure S1. Views of the unit cell of [**1**] as determined by X-ray crystallography data.[29] Faded regions are further from viewpoint. Atom Colors: Cu = brown; O = red; C = grey; N = blue; H = white.

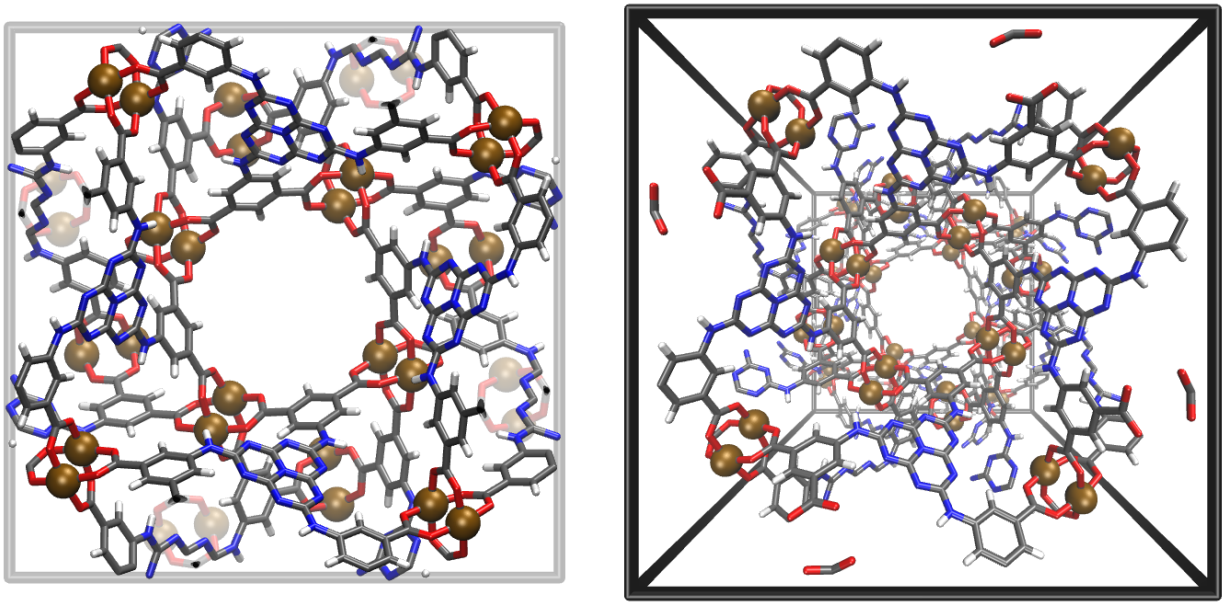

(a) *c*-axis view (orthographic)

(b) *c*-axis view (perspective)

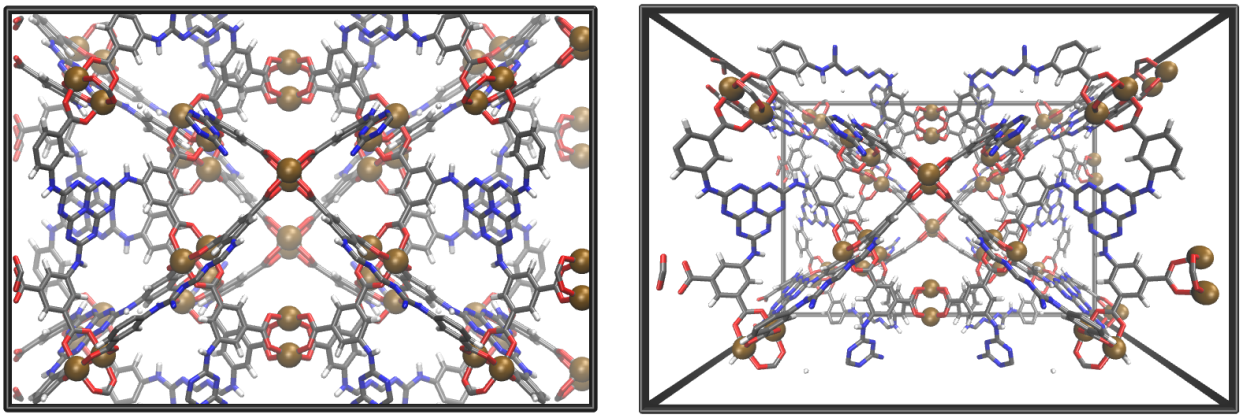

(c) *b*-axis view (orthographic)

(d) *b*-axis view (perspective)

[1] Fragments

Figure S2. Representational gas phase fragments of [**1**] that were selected for charge-fitting calculations. Fragments are displayed with depth-cueing to emphasize dimensionality (faded regions are further from viewpoint). Atom colors: Cu = brown; O = red; C = grey; N = blue; H = white.

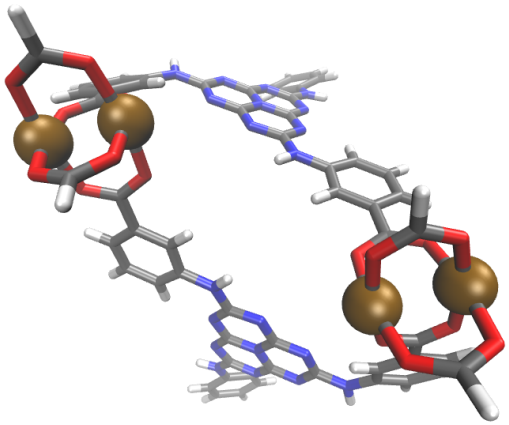

(a) Fragment 1

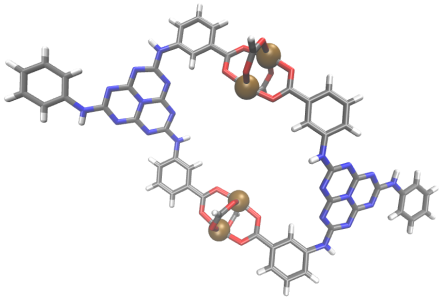

(b) Fragment 2

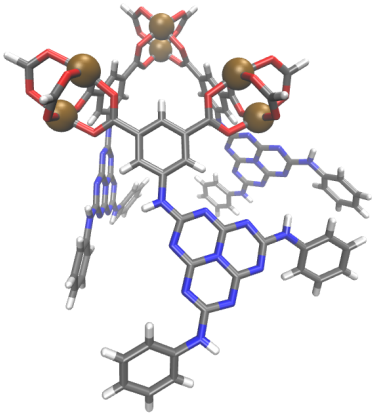

(c) Fragment 3

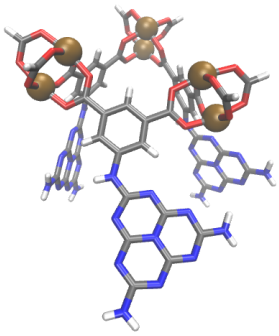

(d) Fragment 4

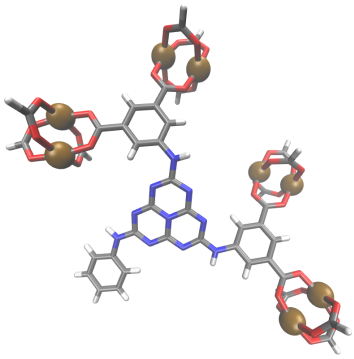

(e) Fragment 5

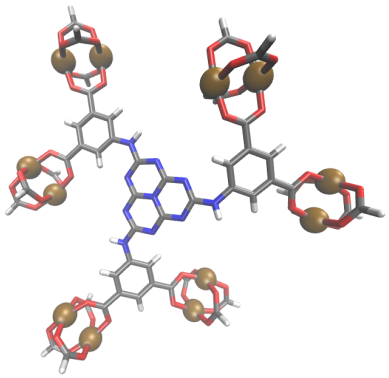

(f) Fragment 6

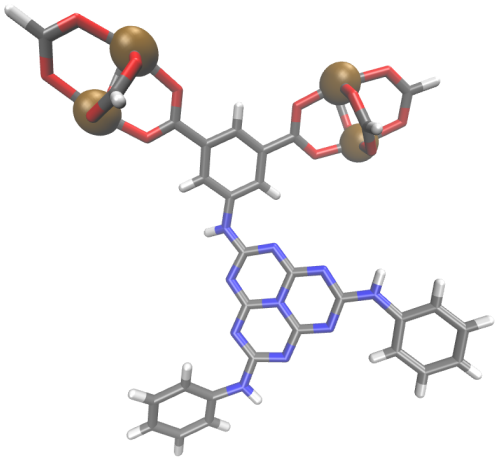

(g) Fragment 7

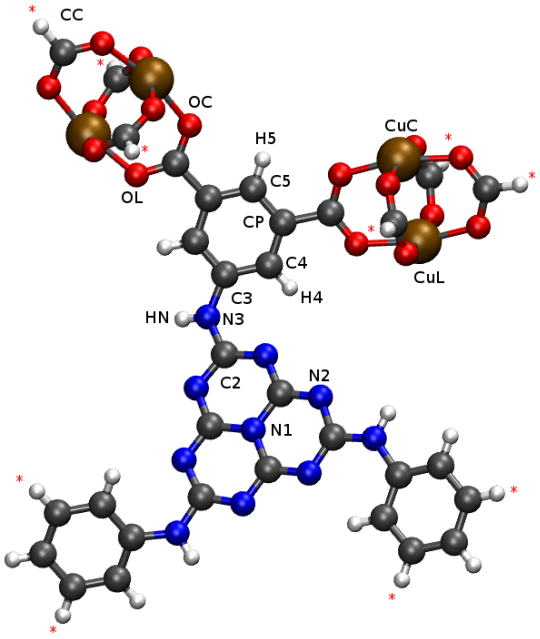

Figure S3. The labels of the chemically distinct atoms in [**1**] as referred to in Table S1. Fragment 7 (Fig. S2(g)) is pictured here. Atom colors: Cu = brown; O = red; C = grey; N = blue; H = white.

Table S1. Average calculated partial charges (in e^-) for the chemically distinct atoms in [**1**], used to parameterize the MOF. These results were obtained as the average of charges calculated from each of the fragments in Fig. S2, using Orca[20] with the Hartree-Fock method[30] using 6-31G* basis sets[31] for all atoms. Labeling of atoms correspond to Figure S3.

Atom #	Atom ID	# in unit-cell	q (e^-)	S.D.
1	CuC	24	1.30649	0.067
2	CuL	24	1.43076	0.048
3	CC	96	1.04239	0.027
4	OC	96	-0.81156	0.007
5	OL	96	-0.81941	0.002
6	CP	96	-0.14003	0.033
7	C1	48	1.05028	0.008
8	C2	48	1.06375	0.025
9	C3	48	0.42570	0.017
10	C4	96	-0.27188	0.031
11	C5	48	-0.16332	0.018
12	N1	16	-0.7866450	0.013
13	N2	96	-0.88286	0.006
14	N3	48	-0.78210	0.005
15	H4	96	0.21926	0.007
16	H5	48	0.19391	0.013
17	HN	48	0.43355	0.001
	Total:	1072		

Table S2. Average charges for individual atoms by fragment in [**1**].

#	Atom Label	Fragment 1	Fragment 2	Fragment 3	Fragment 4	Fragment 5	Fragment 6	Fragment 7
1	CuC	1.36790	1.17275	1.30237	1.31070	1.29725	1.33848	1.35600
2	CuL	1.36085	1.50575	1.42043	1.41417	1.45273	1.43065	1.40750
3	CC	1.02953	1.08800	1.01530	1.02035	1.05330	1.04788	0.98173
4	OC	-0.81438	-0.79361	-0.79971	-0.80393	-0.80469	-0.80233	-0.80534
5	OL	-0.81034	-0.80865	-0.81220	-0.81248	-0.80951	-0.81209	-0.81595
6	CP	-0.09803	-0.18463	-0.11285	-0.11635	-0.14393	-0.13760	-0.17665
7	C1	1.04447	1.04625	1.03829	1.06016	1.05357	1.05353	1.05573
8	C2	1.05673	1.05570	1.05353	1.12091	1.05420	1.04780	1.05737
9	C3	0.43868	0.43293	0.43259	0.41257	0.42860	0.39430	0.44023
10	C4	-0.32218	-0.27498	-0.27250	-0.27420	-0.26165	-0.26062	-0.21720
11	C5	-0.18365	-0.16885	-0.17217	-0.17103	-0.15115	-0.15387	-0.13060
12	N1	-0.76905	-0.77115	-0.75797	-0.79857	-0.78430	-0.78190	-0.78670
13	N2	-0.87176	-0.87190	-0.86944	-0.88664	-0.87175	-0.86910	-0.87507
14	N3	-0.77368	-0.77957	-0.77178	-0.77547	-0.77620	-0.76387	-0.77713
15	H4	0.21525	0.20906	0.21544	0.22907	0.22247	0.22672	0.21682
16	H5	0.18823	0.17990	0.18284	0.21053	0.20710	0.20323	0.18553
17	HN	0.43270	0.43502	0.43150	0.43253	0.43490	0.43323	0.43500

Table S3. Force-field parameters used in MPMC[7] for H_2: Buch[32], BSS[33], BSSP[33], and Darkrim-Levesque[34]. The latter columns are q = charge; α = polarizability; ϵ = Lennard-Jones epsilon; σ = Lennard-Jones sigma.

Model	Site Name	x (Å)	y (Å)	z (Å)	Mass (amu)	q (e)	α (Å^3)	ϵ (K)	σ (Å)
H_2									
BUCH	H2G	0.00000	0.00000	0.00000	2.01600	0.00000	0.00000	34.20000	2.96000
	H2G	0.00000	0.00000	0.00000	0.00000	-0.74640	0.00000	8.85160	3.22930
	H2E	-0.37100	0.00000	0.00000	1.00800	0.37320	0.00000	0.00000	0.00000
BSS	H2E	0.37100	0.00000	0.00000	1.00800	0.37320	0.00000	0.00000	0.00000
	H2N	0.32900	0.00000	0.00000	0.00000	0.00000	0.00000	4.06590	2.34060
	H2N	-0.32900	0.00000	0.00000	0.00000	0.00000	0.00000	4.06590	2.34060
	H2G	0.00000	0.00000	0.00000	0.00000	-0.74640	0.69380	12.76532	3.15528
	H2E	0.37100	0.00000	0.00000	1.00800	0.37320	0.00044	0.00000	0.00000
BSSP	H2E	-0.37100	0.00000	0.00000	1.00800	0.37320	0.00044	0.00000	0.00000
	H2N	0.36300	0.00000	0.00000	0.00000	0.00000	0.00000	2.16726	2.37031
	H2N	-0.36300	0.00000	0.00000	0.00000	0.00000	0.00000	2.16726	2.37031
	H2G	0.00000	0.00000	0.00000	0.00000	-0.93600	0.00000	36.70000	2.95800
DL	H2E	-0.37000	0.00000	0.00000	1.00800	0.46800	0.00000	0.00000	0.00000
	H2E	0.37000	0.00000	0.00000	1.00800	0.46800	0.00000	0.00000	0.00000

Table S4. Force-field parameters used in MPMC[7] for CO_2: PHAST[35], PHAST*[35], and TraPPE[36]. The latter columns are q = charge; α = polarizability; ϵ = Lennard-Jones epsilon; σ = Lennard-Jones sigma.

Model	Site Name	x (Å)	y (Å)	z (Å)	Mass (amu)	q (e)	α (Å^3)	ϵ (K)	σ (Å)
CO_2									
	COG	0.00000	0.00000	0.00000	12.01070	0.77106	0.00000	8.52238	3.05549
	COE	1.16200	0.00000	0.00000	15.99940	-0.38553	0.00000	0.00000	0.00000
PHAST	COE	-1.16200	0.00000	0.00000	15.99940	-0.38553	0.00000	0.00000	0.00000
(nonpolar)	CON	1.09100	0.00000	0.00000	0.00000	0.00000	0.00000	76.76607	2.94473
	CON	-1.09100	0.00000	0.00000	0.00000	0.00000	0.00000	76.76607	2.94473
	COG	0.00000	0.00000	0.00000	12.01070	0.77134	1.22810	19.61757	3.03366
	COE	1.16200	0.00000	0.00000	15.99940	-0.38567	0.73950	0.00000	0.00000
PHAST*	COE	-1.16200	0.00000	0.00000	15.99940	-0.38567	0.73950	0.00000	0.00000
(polar)	CON	1.20800	0.00000	0.00000	0.00000	0.00000	0.00000	46.47457	2.99429
	CON	-1.20800	0.00000	0.00000	0.00000	0.00000	0.00000	46.47457	2.99429
	COG	0.00000	0.00000	0.00000	12.01000	0.70000	0.00000	27.00000	2.80000
TraPPE	COE	1.16000	0.00000	0.00000	16.00000	-0.35000	0.00000	79.00000	3.05000
	COE	-1.16000	0.00000	0.00000	16.00000	-0.35000	0.00000	79.00000	3.05000

Table S5. Force-field parameters used in MPMC[7] for CH_4. The latter columns are q = charge; α = polarizability; ϵ = Lennard-Jones epsilon; σ = Lennard-Jones sigma.

Model	Site Name	x (Å)	y (Å)	z (Å)	Mass (amu)	q (e)	α (Å^3)	ϵ (K)	σ (Å)
CH_4									
TraPPE	CHG	0.00000	0.00000	0.00000	16.04260	0.00000	0.00000	148.00000	3.73000
	CHG	0.00000	0.00000	0.00000	12.01100	-0.58680	0.00000	58.53869	2.22416
	CHE	0.00000	0.00000	1.09900	1.00790	0.14670	0.00000	0.00000	0.00000
	CHE	1.03600	0.00000	-0.36600	1.00790	0.14670	0.00000	0.00000	0.00000
9-site	CHE	-0.51800	-0.89700	-0.36600	1.00790	0.14670	0.00000	0.00000	0.00000
	CHE	-0.51800	0.89700	-0.36600	1.00790	0.14670	0.00000	0.00000	0.00000
	MOV	0.00000	0.00000	0.81600	0.00000	0.00000	0.00000	16.85422	2.96286
	MOV	0.76900	0.00000	-0.27100	0.00000	0.00000	0.00000	16.85422	2.96286
	MOV	-0.38500	-0.66800	-0.27100	0.00000	0.00000	0.00000	16.85422	2.96286
	MOV	-0.38500	0.66800	-0.27100	0.00000	0.00000	0.00000	16.85422	2.96286
	CHG	0.00000	0.00000	0.00000	12.01100	-0.58680	1.09870	45.09730	2.16247
	CHE	0.00000	0.00000	1.09900	1.00790	0.14670	0.42460	0.00000	0.00000
	CHE	1.03600	0.00000	-0.36600	1.00790	0.14670	0.42460	0.00000	0.00000
9-site*	CHE	-0.51800	-0.89700	-0.36600	1.00790	0.14670	0.42460	0.00000	0.00000
	CHE	-0.51800	0.89700	-0.36600	1.00790	0.14670	0.42460	0.00000	0.00000
	MOV	0.00000	0.00000	0.81400	0.00000	0.00000	0.00000	18.57167	2.94787
	MOV	0.76800	0.00000	-0.27000	0.00000	0.00000	0.00000	18.57167	2.94787
	MOV	-0.38300	-0.66600	-0.27000	0.00000	0.00000	0.00000	18.57167	2.94787
	MOV	-0.38300	0.66600	-0.27000	0.00000	0.00000	0.00000	18.57167	2.94787

Table S6. Force-field parameters used in MPMC[7] for C_2H_2[37,38]. The latter columns are q = charge; α = polarizability; ϵ = Lennard-Jones epsilon; σ = Lennard-Jones sigma.

Model	Site Name	x (Å)	y (Å)	z (Å)	Mass (amu)	q (e)	α (Å^3)	ϵ (K)	σ (Å)
C_2H_2									
	C2G	0.60500	0.00000	0.00000	12.01100	-0.29121	0.00000	81.35021	3.40149
nonpolar	C2G	-0.60500	0.00000	0.00000	12.01100	-0.29121	0.00000	81.35021	3.40149
	H2G	1.66500	0.00000	0.00000	1.00800	0.29121	0.00000	0.00026	4.77683
	H2G	-1.66500	0.00000	0.00000	1.00800	0.29121	0.00000	0.00026	4.77683
	C2G	0.60500	0.00000	0.00000	12.01100	-0.29121	1.55140	70.81797	3.42964
polar	C2G	-0.60500	0.00000	0.00000	12.01100	-0.29121	1.55140	70.81797	3.42964
	H2G	1.66500	0.00000	0.00000	1.00800	0.29121	0.14480	0.00026	4.91793
	H2G	-1.66500	0.00000	0.00000	1.00800	0.29121	0.14480	0.00026	4.91793

Table S7. Force-field parameters used in MPMC[7] for C_2H_4. The latter columns are q = charge; α = polarizability; ϵ = Lennard-Jones epsilon; σ = Lennard-Jones sigma.

Model	Site Name	x (Å)	y (Å)	z (Å)	Mass (amu)	q (e)	α (Å^3)	ϵ (K)	σ (Å)
C_2H_4									
	C2G	0.66600	0.00000	0.00000	12.01100	-0.34772	0.00000	69.08116	3.51622
	C2G	-0.66600	0.00000	0.00000	12.01100	-0.34772	0.00000	69.08116	3.51622
nonpolar	H2G	1.23000	0.92100	0.00000	1.00790	0.17386	0.00000	3.16900	2.41504
	H2G	1.23000	-0.92100	0.00000	1.00790	0.17386	0.00000	3.16900	2.41504
	H2G	-1.23000	0.92100	0.00000	1.00790	0.17386	0.00000	3.16900	2.41504
	H2G	-1.23000	-0.92100	0.00000	1.00790	0.17386	0.00000	3.16900	2.41504
	C2G	0.66600	0.00000	0.00000	12.01100	-0.34772	1.63040	52.22317	3.58174
	C2G	-0.66600	0.00000	0.00000	12.01100	-0.34772	1.63040	52.22317	3.58174
polar	H2G	1.23000	0.92100	0.00000	1.00790	0.17386	0.19000	7.47472	2.26449
	H2G	1.23000	-0.92100	0.00000	1.00790	0.17386	0.19000	7.47472	2.26449
	H2G	-1.23000	0.92100	0.00000	1.00790	0.17386	0.19000	7.47472	2.26449
	H2G	-1.23000	-0.92100	0.00000	1.00790	0.17386	0.19000	7.47472	2.26449
TraPPE	CH2	-0.66500	0.00000	0.00000	14.02200	0.00000	0.00000	85.00000	3.67500
	CH2	0.66500	0.00000	0.00000	14.02200	0.00000	0.00000	85.00000	3.67500

Table S8. Force-field parameters used in MPMC[7] for C_2H_6. The latter columns are q = charge; α = polarizability; ϵ = Lennard-Jones epsilon; σ = Lennard-Jones sigma.

Model	Site Name	x (Å)	y (Å)	z (Å)	Mass (amu)	q (e)	α (Å^3)	ϵ (K)	σ (Å)
C_2H_6									
	C2G	-0.76200	0.00000	0.00000	12.01100	-0.04722	0.00000	141.80885	3.28897
	C2G	0.76200	0.00000	0.00000	12.01100	-0.04722	0.00000	141.80885	3.28897
	H2G	-1.15600	1.01500	0.00000	1.00790	0.01574	0.00000	0.62069	2.88406
nonpolar	H2G	-1.15600	-0.50800	0.87900	1.00790	0.01574	0.00000	0.62069	2.88406
	H2G	-1.15600	-0.50800	-0.87900	1.00790	0.01574	0.00000	0.62069	2.88406
	H2G	1.15600	0.50800	0.87900	1.00790	0.01574	0.00000	0.62069	2.88406
	H2G	1.15600	0.50800	-0.87900	1.00790	0.01574	0.00000	0.62069	2.88406
	H2G	1.15600	-1.01500	0.00000	1.00790	0.01574	0.00000	0.62069	2.88406
	C2G	-0.76200	0.00000	0.00000	12.01100	-0.04722	0.69670	98.63326	3.37151
	C2G	0.76200	0.00000	0.00000	12.01100	-0.04722	0.69670	98.63326	3.37151
	H2G	-1.15600	1.01500	0.00000	1.00790	0.01574	0.47580	2.60236	2.57302
polar	H2G	-1.15600	-0.50800	0.87900	1.00790	0.01574	0.47580	2.60236	2.57302
	H2G	-1.15600	-0.50800	-0.87900	1.00790	0.01574	0.47580	2.60236	2.57302
	H2G	1.15600	0.50800	0.87900	1.00790	0.01574	0.47580	2.60236	2.57302
	H2G	1.15600	0.50800	-0.87900	1.00790	0.01574	0.47580	2.60236	2.57302
	H2G	1.15600	-1.01500	0.00000	1.00790	0.01574	0.47580	2.60236	2.57302
TraPPE	CH3	0.77000	0.00000	0.00000	15.0350	0.00000	0.00000	98.00000	3.75000
	CH3	-0.77000	0.00000	0.00000	15.0350	0.00000	0.00000	98.00000	3.75000

H_2 Sorption Details

Figure S4. Equilibrium H_2 gas occupation (shown in green) in [**1**] from BSSP simulation at 77 K and 0.05 atm. Views are (a) down *a*-axis and (b) *c*-axis and of the unit cell. View (c) is zoomed to the secondary sorption site, which is nestled in the corner of the truncated tetrahedron (T-T_d). Isovalue = 0.002; Resolution of bins = 0.7 Å. Figures shown with depth-cueing to emphasize dimensionality (faded atoms are further from viewpoint). Atom colors: Cu=brown; C=grey; N=blue; O=red; H=white. Note, the highest occupancies occur near CuL.

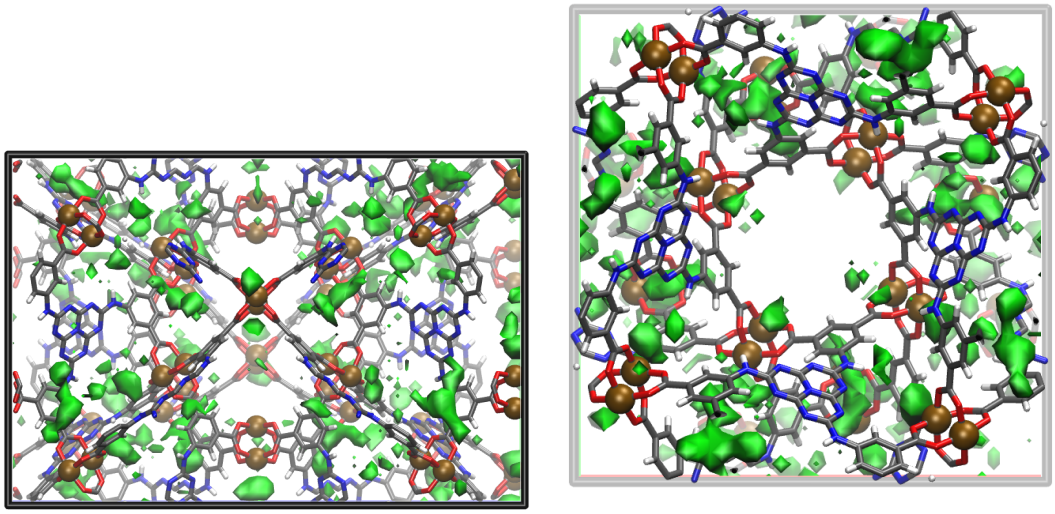

(a) (b)

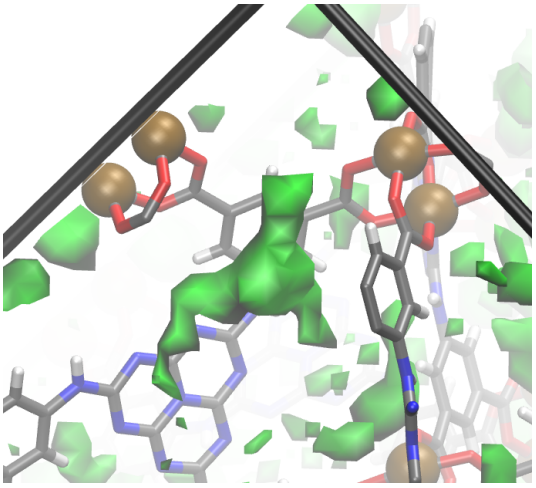

(c)

Figure S5. H_2 dipole distributions for BSSP model at 77 K. Note the small, broad peak in the range 0.15 – 0.35 Debye, which corresponds to strong polarization interaction between H_2 molecules and [**1**].

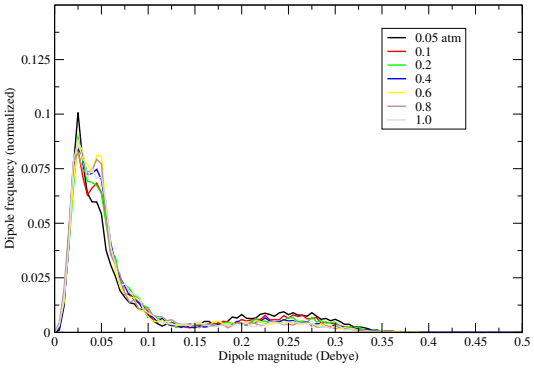

Figure S6. Equilibrated percent total energy contributions of repulsion/dispersion, electrostatic, and polarization energies for the BSSP model at 77 K as a function of pressure. Note, while repulsion/dispersion energy dominates the system quantitatively, only the polar model yields open-metal sorption detection.

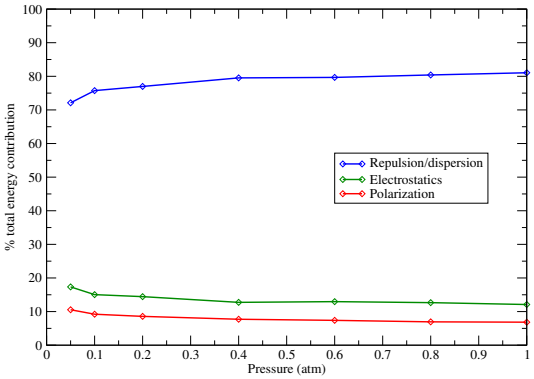

Figure S7. Radial distribution of copper charge-swap test, where CuC and CuL charges were swapped and simulations ran for the BSSP model at 77 K and 0.05atm. (a) shows CuC – H_2 distances, (b) shows CuL – H_2 distances. Black = original parametrization (CuC=1.31; CuL=1.43); Red = swapped parametrization (CuC=1.43; CuL=1.31).

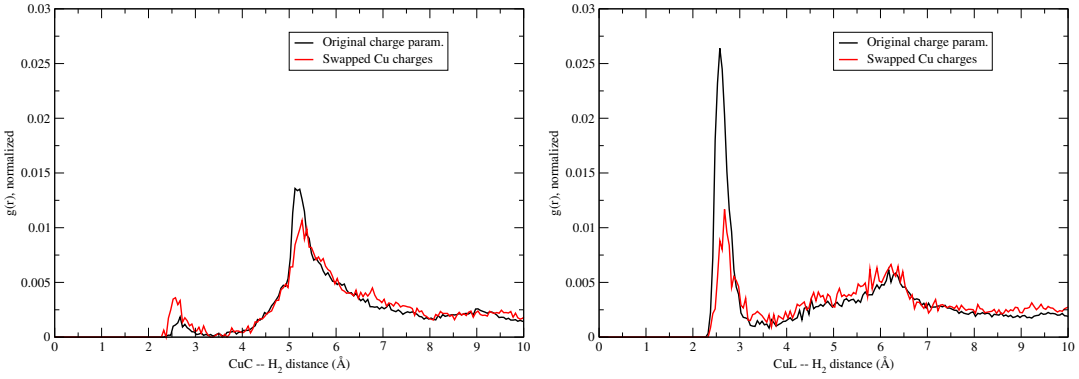

(a) (b)

Figure S8. Locations of H_2 (a) strongest (0.175 – 0.50 D; pink) dipoles with (b) rotated view 90° in y and (c) weaker (0.05 – 0.175 D; purple) dipoles with (d) rotated view 90° in y. Taken from the equilibrated BSSP model for H_2 at 77 K and 0.05 atm. Figures shown with depth-cueing to emphasize dimensionality (faded atoms are further from viewpoint). Atom colors: CuC=green; CuL=orange; C=grey; N=blue; O=red; H=white. Note, the strongest dipoles occur near CuL.

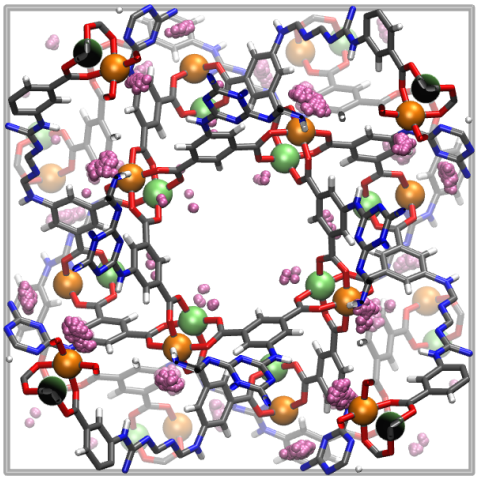

(a)

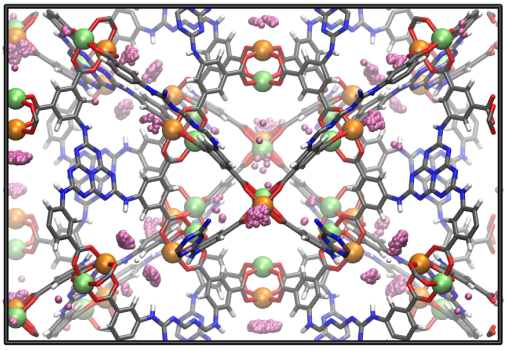

(b)

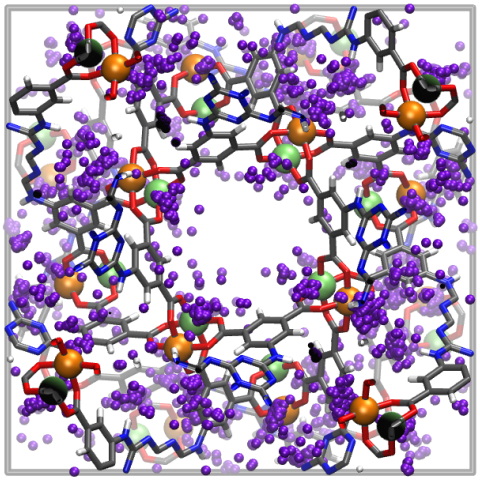

(c)

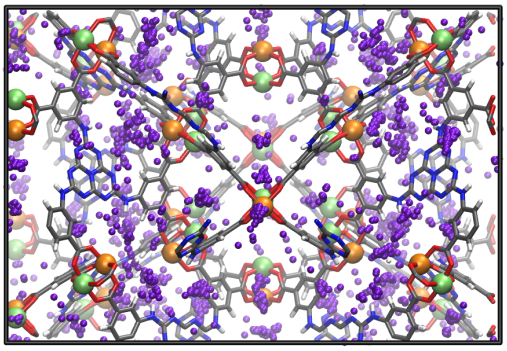

(d)

Figure S9. Sorption sites for (a) BSSP (site 1), (b) BSS (site 3) and (c) DL (site 4) for H_2 as revealed by simulated annealing. The H_2 C.O.M. – CuL distance for (a) is 2.68 Å.

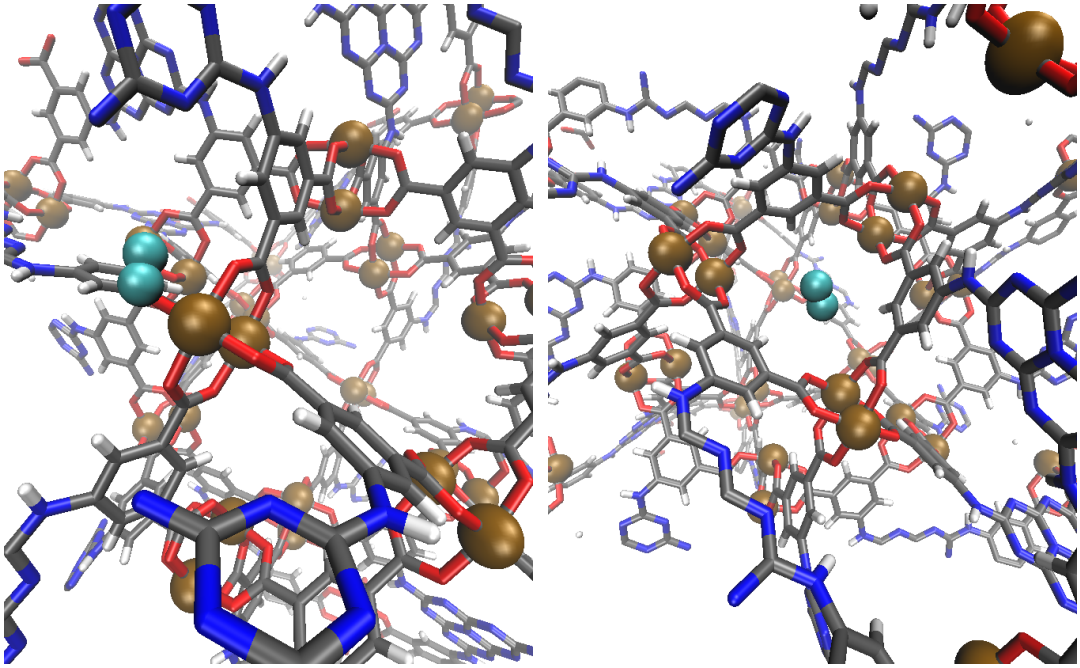

(a) (b)

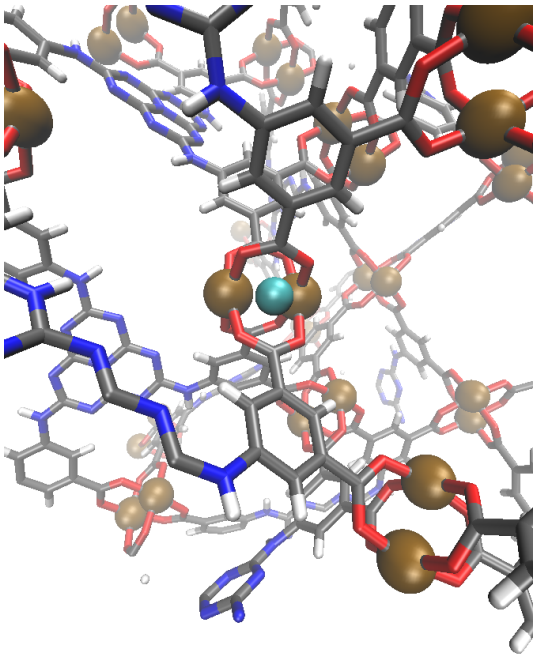

(c)

CO_2 Sorption Details

Figure S10. Equilibrium CO_2 gas occupation (shown in green) in [**1**] from polar simulation at 298 K and 0.05 atm. Views are (a) down *a*-axis and (b) *c*-axis and of the unit cell. View (c) is zoomed to the sorption sites, in this case at CuL and in the corner site, which is nestled in the corner of the truncated tetrahedron (T-T_d). Isovalue = 0.00002; Resolution of bins = 0.7 Å. Figures shown with depth-cueing to emphasize dimensionality (faded atoms are further from viewpoint). Atom colors: Cu=brown; C=grey; N=blue; O=red; H=white.

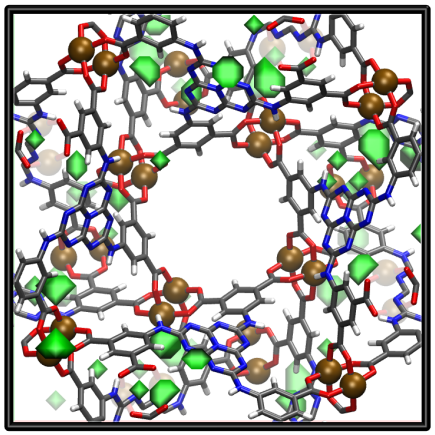

(a)

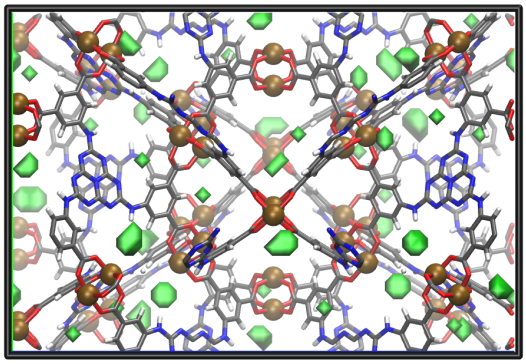

(b)

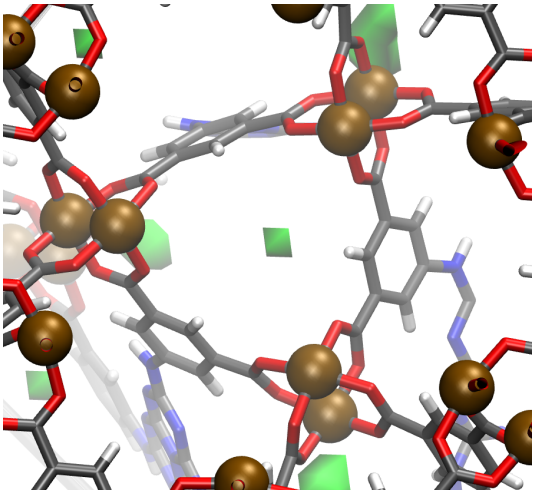

(c)

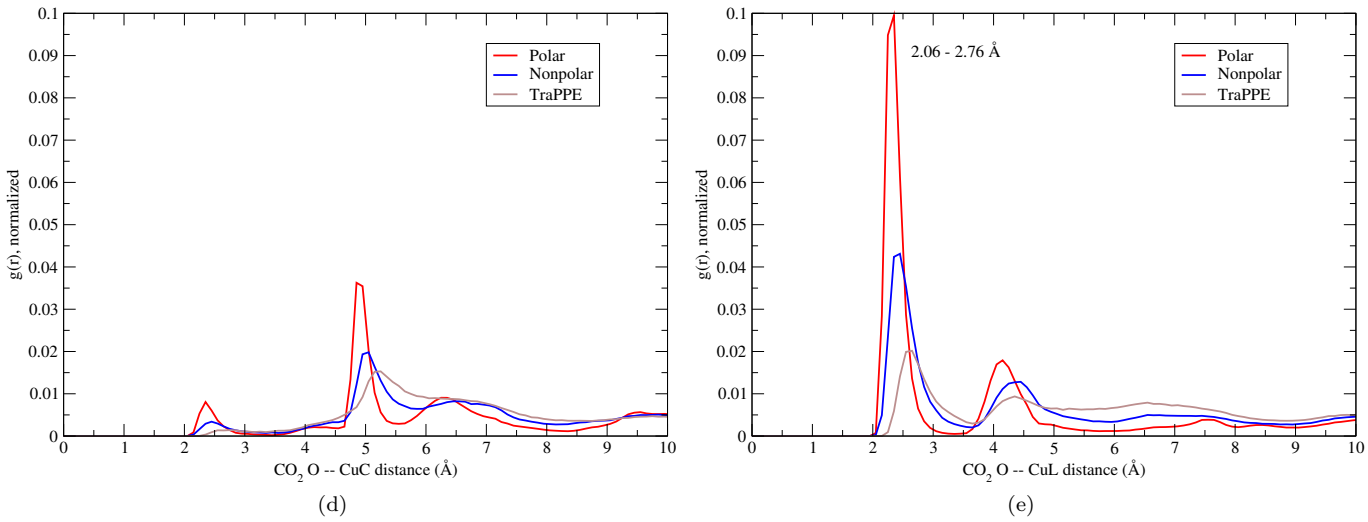

Figure S11. Radial distribution of CO_2 **oxygen** atoms with (a) CuC (the copper facing towards the rhombicuboctahedral cage), and (b) CuL at 298 K and 0.05 atm. Red = polar model; blue = nonpolar; brown = TraPPE.

Figure S12. CO_2 dipole distributions for polar model at 298 K.

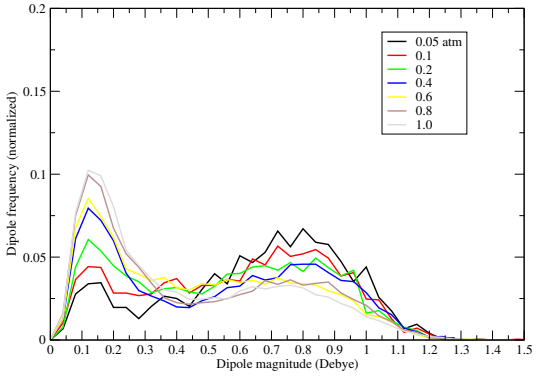

Figure S13. Equilibrated percent total energy contributions of repulsion/dispersion, electrostatic, and polarization energies for the CO_2 polar (PHAST*) model at 298 K as a function of pressure.

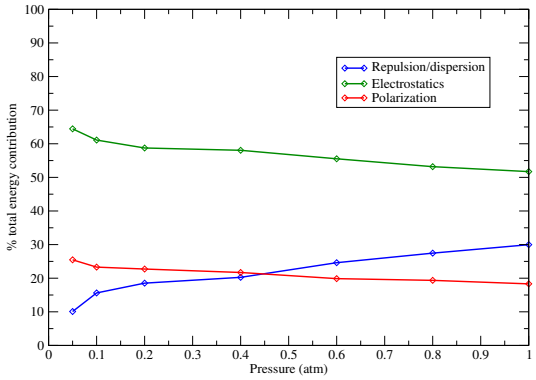

Figure S14. Sorption sites for (a) polar (site 2) and (b) TraPPE (site 1) CO_2 as revealed by simulated annealing. The CuC – C distance for (a) is 3.06 Å, and the CuL – C distance for (b) is 3.36 Å.

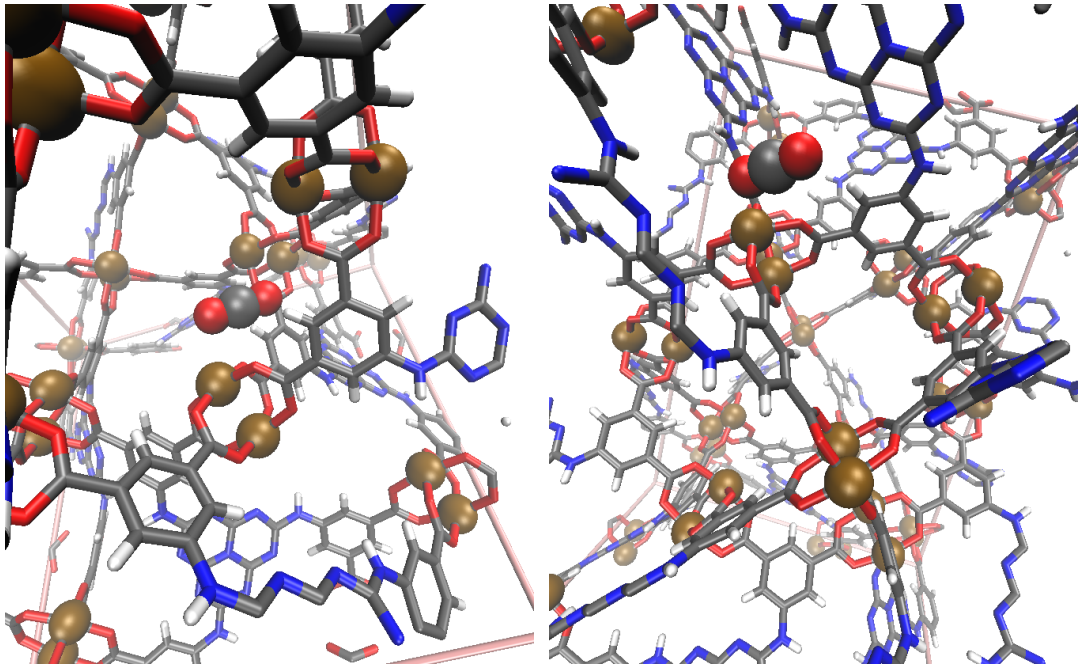

(a) (b)

CH_4 Sorption Details

Figure S15. Equilibrium CH_4 gas occupation (shown in green) in [**1**] from polarized simulation at 298 K and 0.05 atm. The views are centered, at different angles, on the only observed sorption site for CH_4 (compare with Fig. S4(c)), which is nestled in the corner of the truncated tetrahedron (T-T_d). Isovalue = 0.002; Resolution of bins = 0.7 Å. Figures shown with depth-cueing to emphasize dimensionality (faded atoms are further from viewpoint). Atom colors: Cu=brown; C=grey; N=blue; O=red; H=white. Note, no other sorption site is evident even up to 1.0 atm for other models.

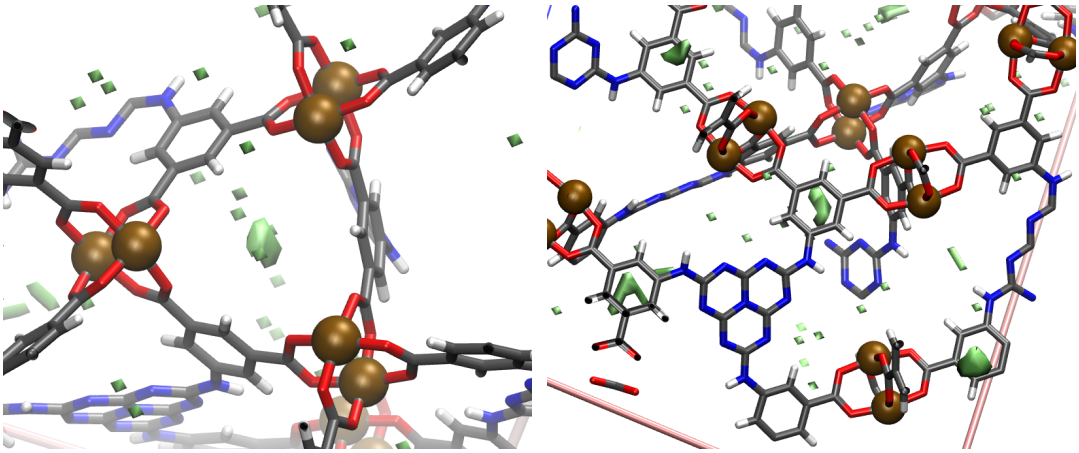

(a) (b)

Figure S16. Calculated Q_{st} (at 298 K) compared with experiment for CH_4. Black = experiment[39]; Red = polar model; Blue = nonpolar model; Brown = TraPPE.

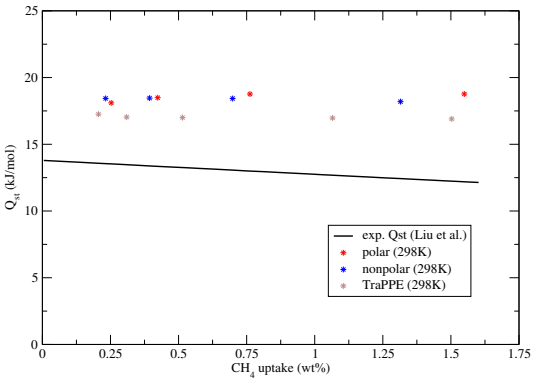

Figure S17. CH_4 dipole distributions for polar model at 298 K.

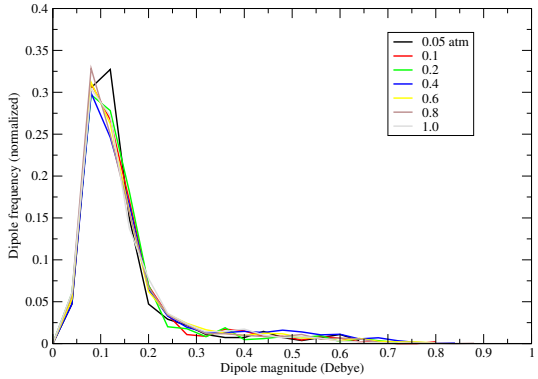

Figure S18. Equilibrated percent total energy contributions of repulsion/dispersion, electrostatic, and polarization energies for the CH_4 9-site polar model at 298 K as a function of pressure.

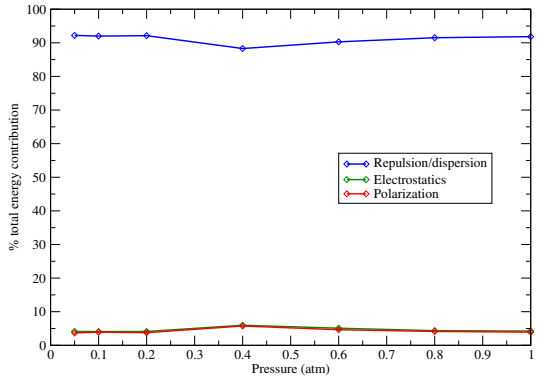

Figure S19. Radial distribution of CH_4 center-of-mass about (a) CuC and (b) CuL at 0.05atm and 298K. Red = polar model; Blue = nonpolar model; Brown = TraPPE model.

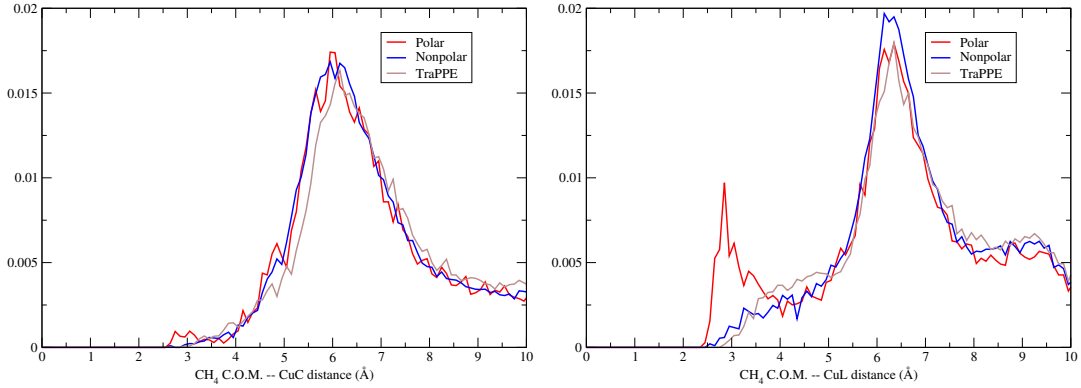

(a) (b)

Figure S20. Sorption sites for (a) polar (site 4) and (b) nonpolar (site 3) CH_4 as revealed by simulated annealing.

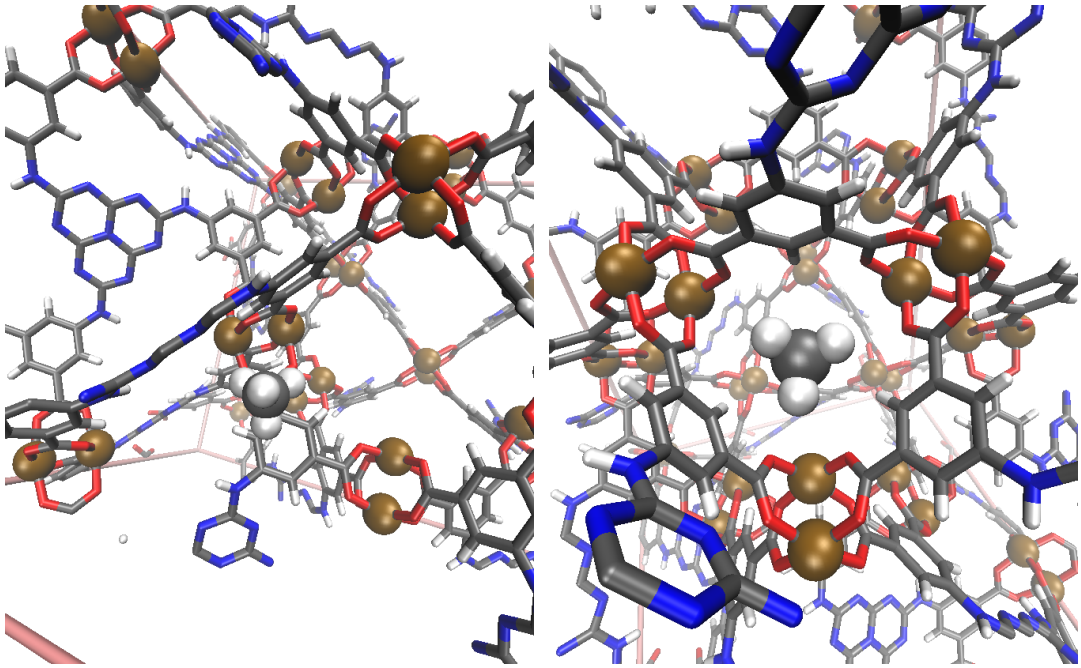

(a) (b)

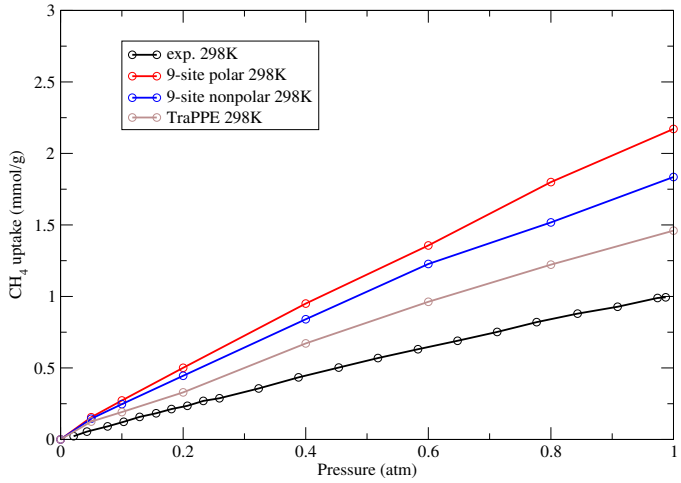

Figure S21. CH_4 adsorption at 298 K from 0 to 1 atm. Black = experiment[39]; Red = polar model; blue = nonpolar; brown = TraPPE.

C_2H_2 Sorption Details

Figure S22. Equilibrium C_2H_2 gas occupation (shown in green) in [**1**] from polar simulation at 298 K and 0.05 atm. Views are (a) down *a*-axis and (b) *c*-axis and of the unit cell. View (c) is zoomed to the sorption sites, in this case at CuC, CuL, and in the corner site, which is nestled in the corner of the truncated tetrahedron (T-T_d). Isovalue = 0.0005; Resolution of bins = 0.7 Å. Figures shown with depth-cueing to emphasize dimensionality (faded atoms are further from viewpoint). Atom colors: Cu=brown; C=grey; N=blue; O=red; H=white.

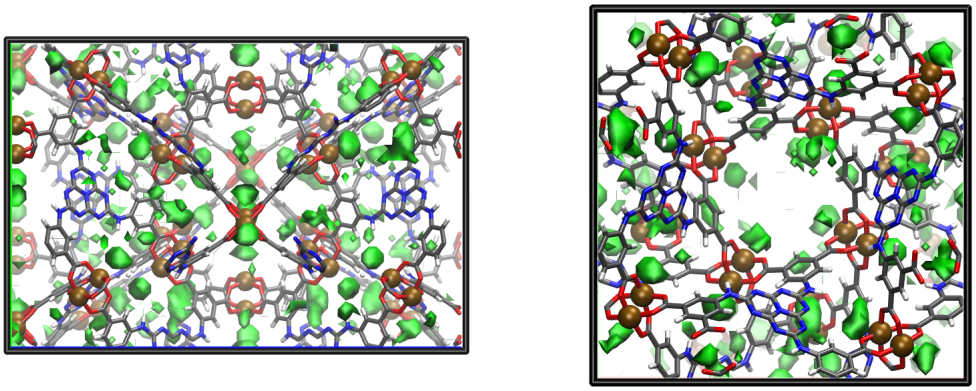

(a) (b)

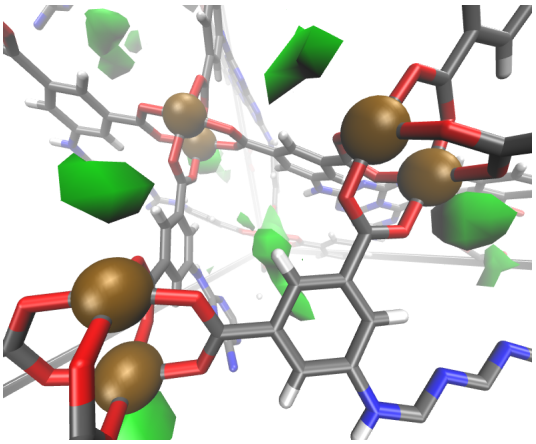

(c)

Figure S23. Calculated Q_{st} (at 298 K) compared with experiment for C_2H_2. Black = experiment[39]; Red = polar model; Blue = nonpolar model.

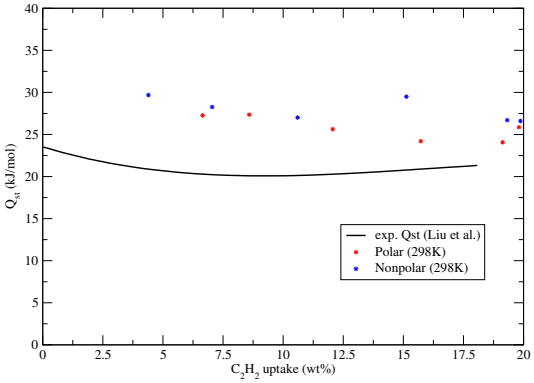

Figure S24. C_2H_2 dipole distributions for polar model at 298 K. Note, the effect of increasing pressure leads to weaker dipoles throughout the MOF–sorbate system, and the dipole strengths of these systems are ~4× those of the corresponding H_2 systems (Fig. S12).

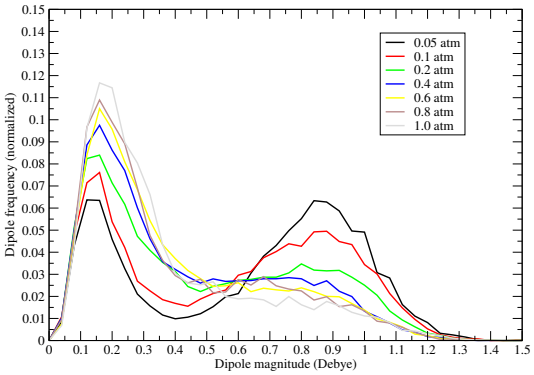

Figure S25. Equilibrated percent total energy contributions of repulsion/dispersion, electrostatic, and polarization energies for the C_2H_2 polar model at 298 K as a function of pressure.

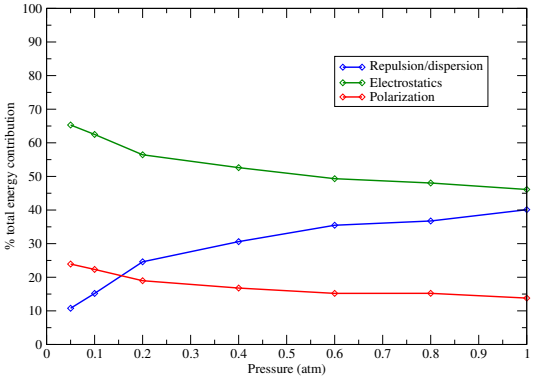

Figure S26. Radial distribution of C_2H_2 carbon atoms about (a) CuC and (b) CuL at 0.05atm and 298K. Red = polar model; Blue = nonpolar model.

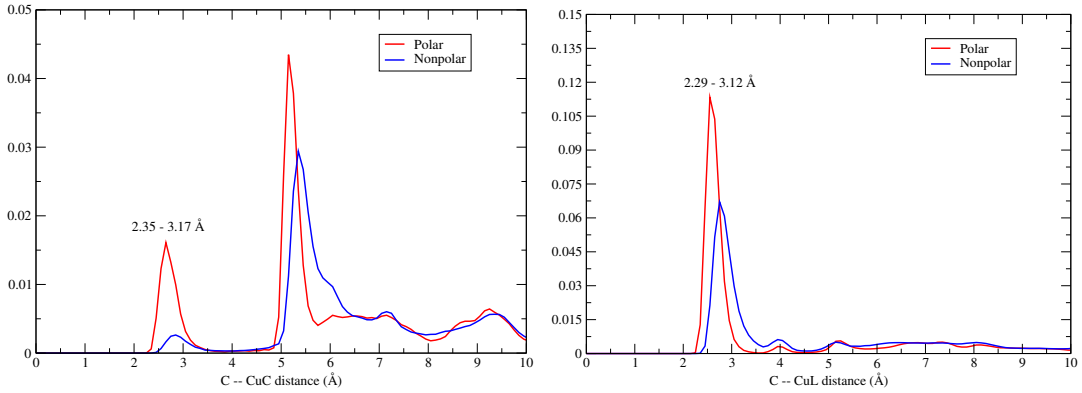

Figure S27. Sorption site for nonpolar C_2H_2 as revealed by simulated annealing at site 2 (CuC). Here, the CuC – C distance is 2.63 Å.

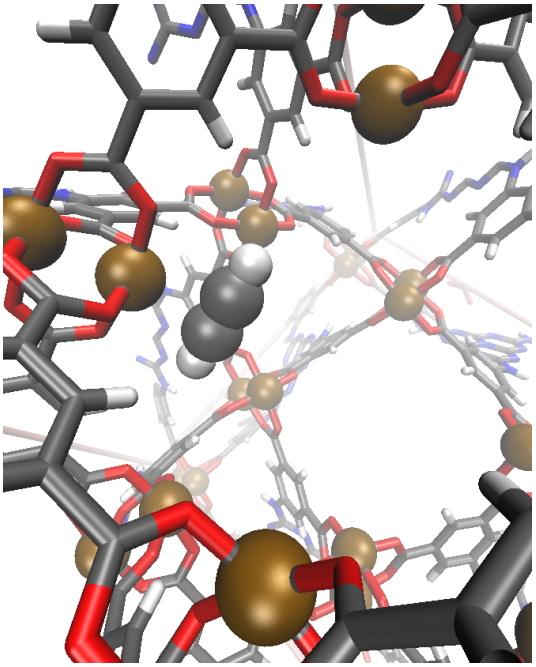

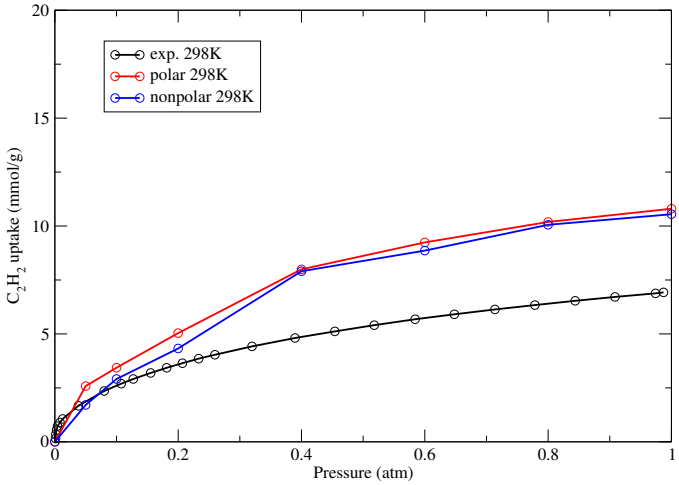

Figure S28. C_2H_2 adsorption at 298 K from 0 to 1 atm. Black = experiment[39]; Red = polar model; blue = nonpolar.

C_2H_4 Sorption Details

Figure S29. Equilibrium C_2H_4 gas occupation (shown in green) in [**1**] from polar simulation at 298 K and 0.05 atm. Views are (a) down *a*-axis and (b) *c*-axis and of the unit cell. View (c) is zoomed to the sorption sites, in this case at CuC, CuL, and in the corner site, which is nestled in the corner of the truncated tetrahedron (T-T_d). Isovalue = 0.00012; Resolution of bins = 0.7 Å. Figures shown with depth-cueing to emphasize dimensionality (faded atoms are further from viewpoint). Atom colors: Cu=brown; C=grey; N=blue; O=red; H=white.

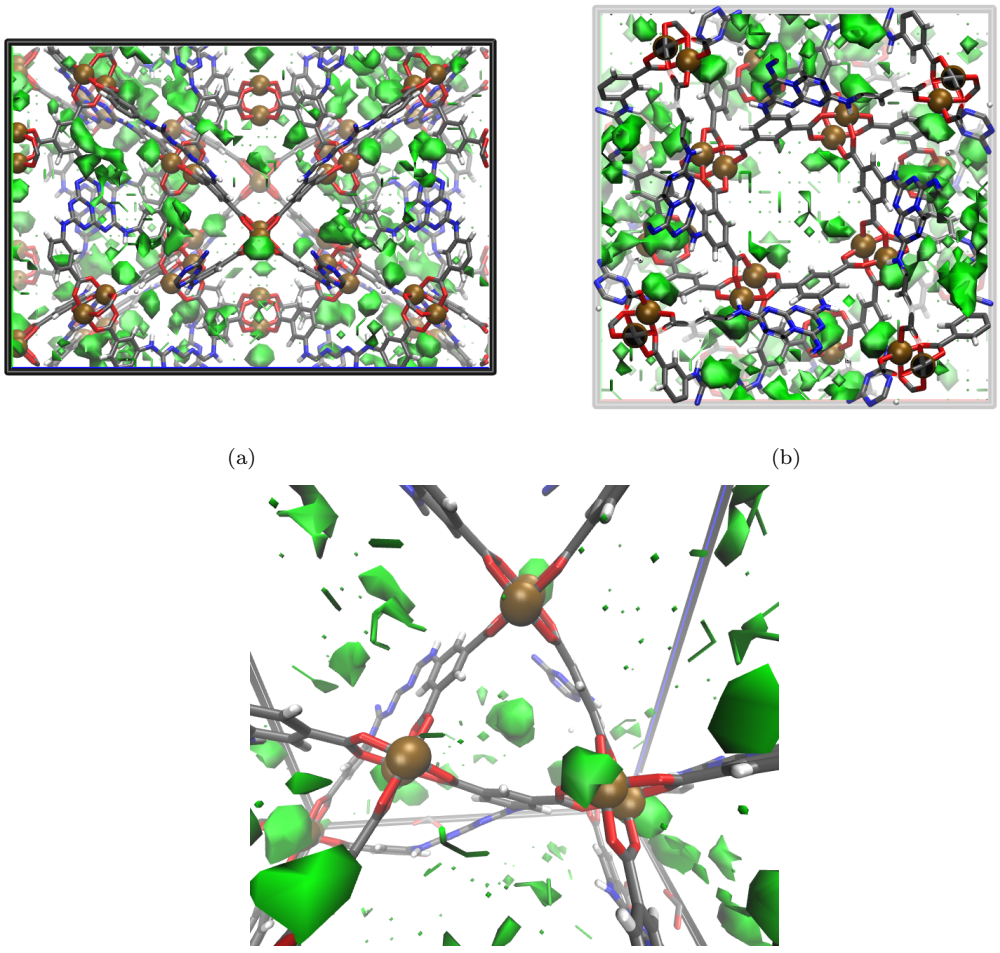

(a) (b)

(c)

Figure S30. Calculated Q_{st} (at 298 K) compared with experiment for C_2H_4. Black = experiment[39]; Red = polar model; Blue = nonpolar model; Brown = TraPPE model.

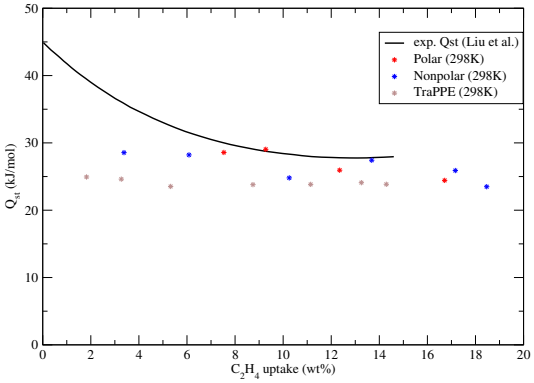

Figure S31. C_2H_4 dipole distributions for polar model at 298 K. Note, the effect of increasing pressure leads to weaker dipoles throughout the MOF–sorbate system.

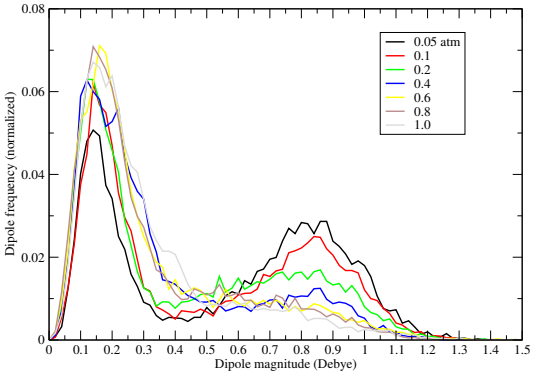

Figure S32. Equilibrated percent total energy contributions of repulsion/dispersion, electrostatic, and polarization energies for the C_2H_4 polar model at 298 K as a function of pressure.

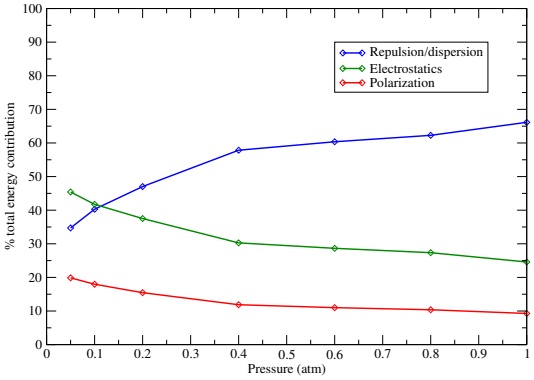

Figure S33. Radial distribution of C_2H_4 carbon atoms about (a) CuC and (b) CuL at 0.05atm and 298K. Red = polar model; Blue = nonpolar model. Brown = TraPPE.

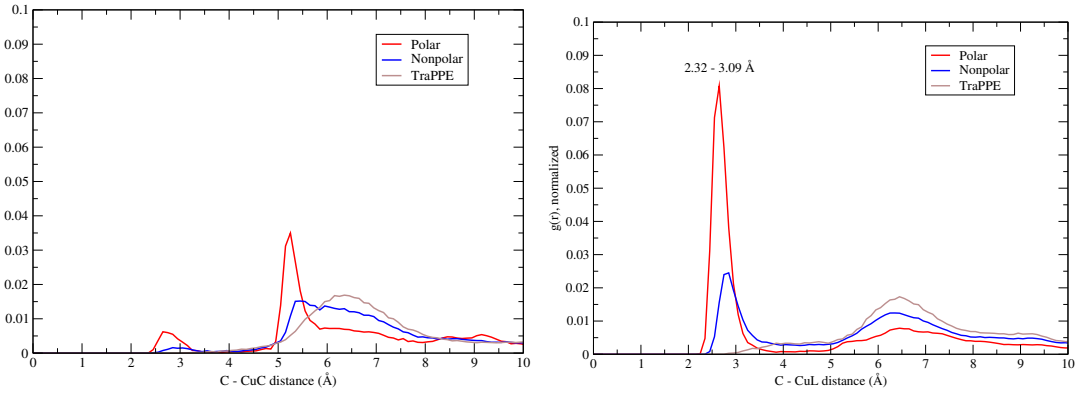

(a) (b)

Figure S34. Sorption sites for (a) polar (site 2, CuC) and (b) nonpolar (site 4) C_2H_4 as revealed by simulated annealing. The CuC – C distance for (a) is 2.62 Å.

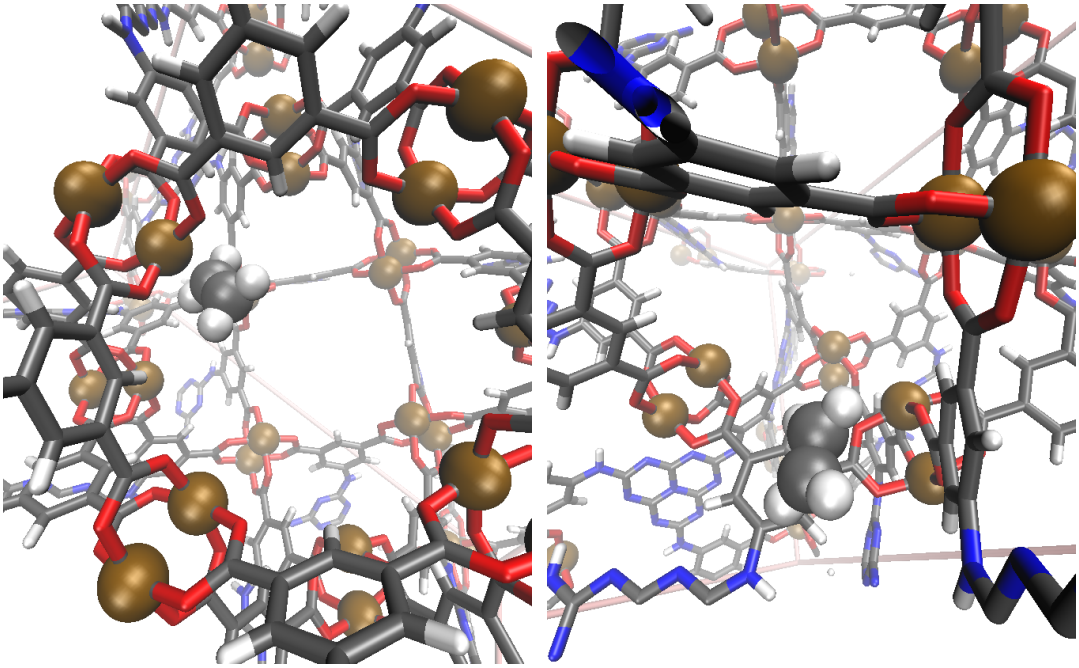

(a) (b)

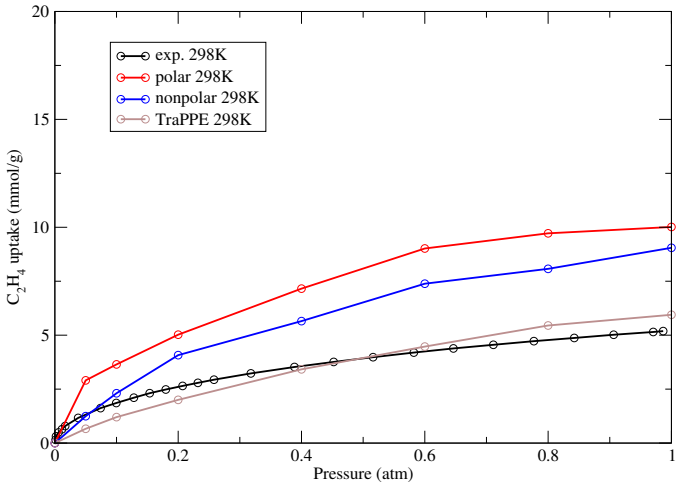

Figure S35. C_2H_4 adsorption at 298 K from 0 to 1 atm. Black = experiment[39]; Red = polar model; blue = nonpolar; brown = TraPPE.

C_2H_6 Sorption Details

Figure S36. Equilibrium C_2H_6 gas occupation (shown in green) in [**1**] from polar simulation at 298 K and 0.05 atm. Views are (a) down *a*-axis and (b) *c*-axis and of the unit cell. View (c) is zoomed to the primary sorption site, which is nestled in the corner of the truncated tetrahedron (T-T_d). Isovalue = 0.00012; Resolution of bins = 0.7 Å. Figures shown with depth-cueing to emphasize dimensionality (faded atoms are further from viewpoint). Atom colors: Cu=brown; C=grey; N=blue; O=red; H=white.

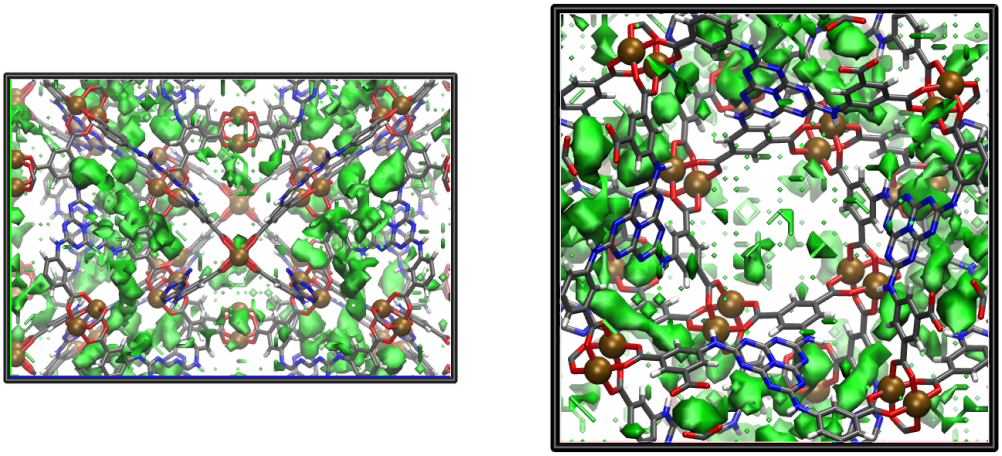

(a) (b)

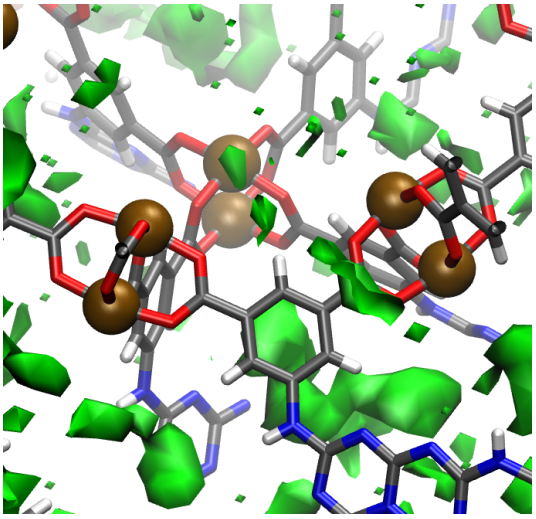

(c)

Figure S37. Calculated Q_{st} (at 298 K) compared with experiment for C_2H_6. Black = experiment[39]; Red = polar model; Blue = nonpolar model; Brown = TraPPE model.

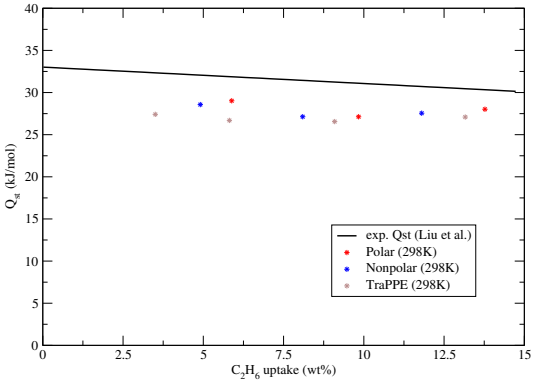

Figure S38. C_2H_6 dipole distributions for polar model at 298 K. Note the lack of strong dipoles compared to other sorbates (Figs S12, S24, and S31).

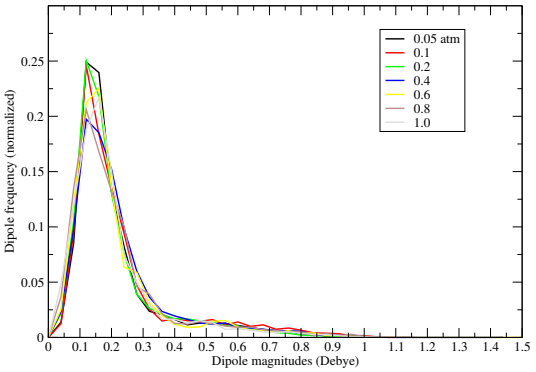

Figure S39. Equilibrated percent total energy contributions of repulsion/dispersion, electrostatic, and polarization energies for the C_2H_6 polar model at 298 K as a function of pressure. Note, the highest electrostatic contribution is 0.164%.

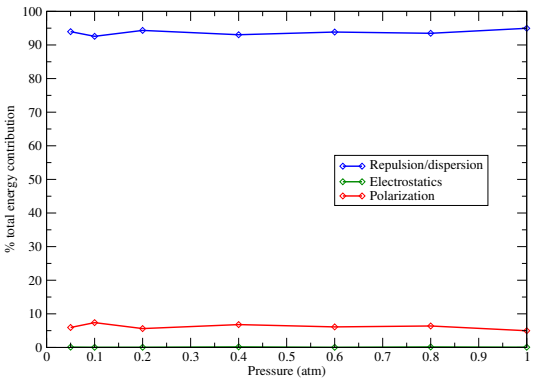

Figure S40. Radial distribution of C_2H_6 carbon atoms about (a) CuC and (b) CuL at 0.05atm and 298K. Red = polar model; Blue = nonpolar model. Brown = TraPPE.

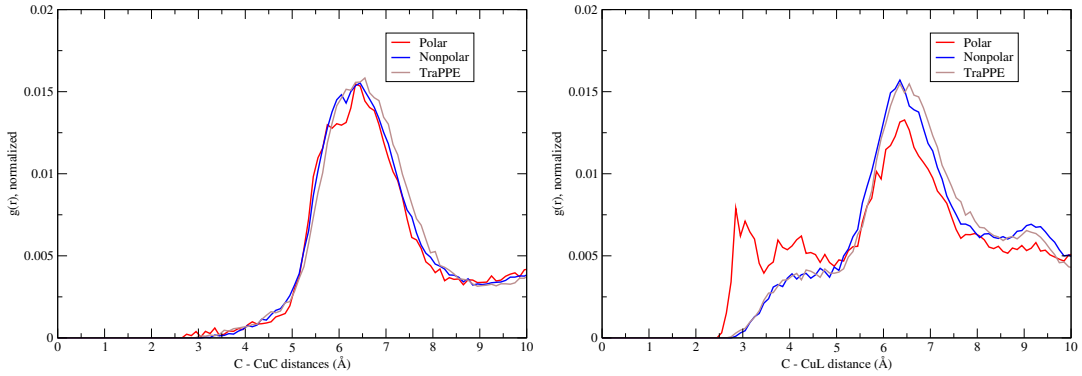

(a) (b)

Figure S41. Sorption (site 4) for C_2H_6 as revealed by simulated annealing.

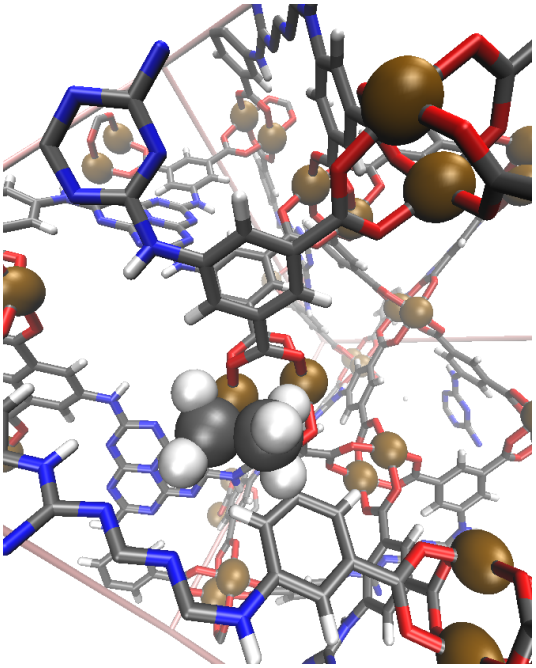

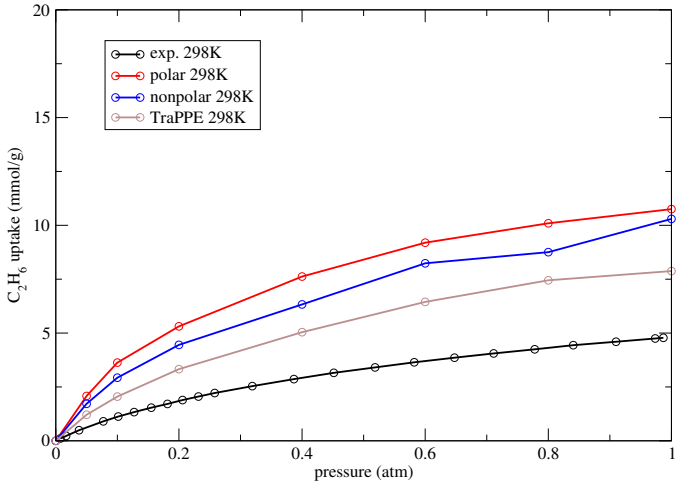

Figure S42. C_2H_6 adsorption at 298 K from 0 to 1 atm. Black = experiment[39]; Red = polar model; blue = nonpolar; brown = TraPPE.

[1] N. Metropolis, A. W. Rosenbluth, M. N. Rosenbluth, A. H. Teller and E. Teller, *J. Chem. Phys.*, 1953, **21**, 1087–1092.
[2] D. A. McQuarrie, *Statistical Mechanics*, University Science Books, Sausalito, CA, 2000.
[3] D. Frenkel and B. Smit, *Understanding Molecular Simulation: From Algorithms to Applications*, Academic Press, New York, 2002.
[4] T. Boublík, *Fluid Phase Equil.*, 2005, **240**, 96–100.
[5] R. P. Feynman and A. R. Hibbs, *Quantum Mechanics and Path Integrals*, McGraw-Hill, New York, 1965.
[6] D. Nicholson and N. G. Parsonage, *Computer Simulation and the Statistical Mechanics of Adsorption*, Academic Press, London, 1982.
[7] J. L. Belof and B. Space, *Massively Parallel Monte Carlo (MPMC)*, Available on GitHub, 2012, `https://github.com/mpmccode/mpmc`.
[8] D. M. Franz, *Monte Carlo - Molecular Dynamics*, Available on GitHub, 2017, `https://github.com/khavernathy/mcmd`.
[9] J. Applequist, J. R. Carl and K.-K. Fung, *J. Am. Chem. Soc.*, 1972, **94**, 2952–2960.
[10] B. Thole, *Chem. Phys.*, 1981, **59**, 341 – 350.
[11] K. A. Bode and J. Applequist, *J. Phys. Chem.*, 1996, **100**, 17820–17824.
[12] T.-L. Dinh and G. A. Huber, *J Math. Modell. Algorithms*, 2005, **4**, 111–128.
[13] J. L. Belof, *Ph.D. thesis*, University of South Florida, 2009.
[14] J. L. Belof, A. C. Stern, M. Eddaoudi and B. Space, *J. Am. Chem. Soc.*, 2007, **129**, 15202–15210.
[15] K. A. Forrest, T. Pham, K. McLaughlin, J. L. Belof, A. C. Stern, M. J. Zaworotko and B. Space, *J. Phys. Chem. C*, 2012, **116**, 15538–15549.
[16] K. Palmo and S. Krimm, *Chem. Phys. Lett.*, 2004, **395**, 133–137.
[17] W. Humphrey, A. Dalke and K. Schulten, *Journal of molecular graphics*, 1996, **14**, 33–38.
[18] S. Kirkpatrick, J. C.D. Gelatt and M. Vecchi, *Science*, 1983, **220**, 671–680.
[19] T. H. Dunning Jr, *The Journal of chemical physics*, 1989, **90**, 1007–1023.
[20] F. Neese, *WIREs Comput. Mol. Sci.*, 2012, **2**, 73–78.
[21] C. M. Breneman and K. B. Wiberg, *J. Comput. Chem.*, 1990, **11**, 361–373.
[22] C. D. Sherrill, A. I. Krylov, E. F. Byrd and M. Head-Gordon, *The Journal of chemical physics*, 1998, **109**, 4171–4181.
[23] A. Misquitta and A. Stone, *University of Cambridge*, 2007.
[24] M. E. Casida and D. R. Salahub, *The Journal of Chemical Physics*, 2000, **113**, 8918–8935.
[25] M. Valiev, E. Bylaska, N. Govind, K. Kowalski, T. Straatsma, H. V. Dam, D. Wang, J. Nieplocha, E. Apra, T. Windus and W. de Jong, *Comput. Phys. Commun.*, 2010, **181**, 1477 – 1489.
[26] C. Ruth Le Sueur and A. J. Stone, *Molecular Physics*, 1994, **83**, 293–307.
[27] D. G. Truhlar, *Chemical Physics Letters*, 1998, **294**, 45–48.
[28] S. F. Boys and F. d. Bernardi, *Molecular Physics*, 1970, **19**, 553–566.
[29] R. Luebke, L. Weselinski, Y. Belmabkhout, Z. Chen, L. Wojtas and M. Eddaoudi, *Cryst. Growth Des.*, 2014, **14**, 414–418.
[30] J. C. Slater, *Physical Review*, 1951, **81**, 385.
[31] W. J. Hehre, R. Ditchfield and J. A. Pople, *The Journal of Chemical Physics*, 1972, **56**, 2257–2261.
[32] V. Buch, *J. Chem. Phys.*, 1994, **100**, 7610–7629.
[33] J. L. Belof, A. C. Stern and B. Space, *J. Chem. Theory Comput.*, 2008, **4**, 1332–1337.
[34] F. Darkrim and D. Levesque, *J. Chem. Phys.*, 1998, **109**, 4981.
[35] A. L. Mullen, T. Pham, K. A. Forrest, C. R. Cioce, K. McLaughlin and B. Space, *J. Chem. Theory Comput.*, 2013, **9**, 5421–5429.
[36] J. J. Potoff and J. I. Siepmann, *AIChE J.*, 2001, **47**, 1676–1682.
[37] K.-J. Chen, H. S. Scott, D. G. Madden, T. Pham, A. Kumar, A. Bajpai, M. Lusi, K. A. Forrest, B. Space and J. J. Perry, *Chem*, 2016, **1**, 753–765.
[38] H. S. Scott, M. Shivanna, A. Bajpai, D. G. Madden, K.-J. Chen, T. Pham, K. A. Forrest, A. Hogan, B. Space and J. J. Perry IV, *ACS Appl. Mater. Interfaces*, 2017.
[39] K. Liu, B. Li, Y. Li, X. Li, F. Yang, G. Zeng, Y. Peng, Z. Zhang, G. Li and Z. Shi, *Chem. Commun.*, 2014, **50**, 5031–5033.